

Synthesis of the nickel selenophosphinates $[\text{Ni}(\text{Se}_2\text{PR}_2)_2]$ ($\text{R} = {}^i\text{Pr}, {}^t\text{Bu}$ and Ph) and their use as single source precursors for the deposition of nickel phosphide or nickel selenide nanoparticles†

Weerakanya Maneepakorn, Chinh Q. Nguyen, Mohammad A. Malik, Paul O'Brien* and James Raftery

Received 29th September 2008, Accepted 9th January 2009

First published as an Advance Article on the web 5th February 2009

DOI: 10.1039/b816903a

Nickel phosphide (Ni_3P and Ni_{12}P_5) or nickel selenide (NiSe) nanoparticles were prepared from the single molecule precursor, dialkyldiselenophosphinato nickel(II), $[\text{Ni}(\text{Se}_2\text{PR}_2)_2]$ ($\text{R} = {}^i\text{Pr}, {}^t\text{Bu}$ and Ph) by thermolysis in trioctylphosphine oxide (TOPO) or hexadecylamine (HDA). The chemical composition of these nanoparticles depends on the precursors, capping agents, and reaction temperature.

Introduction

Nickel phosphides are excellent corrosion-resistant, oxidation-resistant and waterproofing materials.¹ Nanocrystalline phosphides have distinctive mechanical and thermal properties. Previous studies, and the calculated Ni-P binary phase diagram, indicate that the possible nickel phosphide phases are: Ni_3P , Ni_{12}P_5 , Ni_3P_2 , and Ni_2P .² Nickel phosphide is an n-type semiconductor with a band gap of 1.0 eV.³ There are very few reports on the preparation of nickel phosphide nanoparticles; most of these, use a phosphine. The phosphide was prepared by the direct reaction between phosphine (PH_3) and the metal or metal salts.⁴ It was also reported that nickel phosphide particles can be easily prepared from metal or metal oxide on a silica-support by reaction with PH_3 .⁵ Recently, spherical metal phosphide nanoparticles were synthesised by the reaction of metal carbonyl complexes with phosphine. In this case, the phosphine surfactant can serve as both stabilising ligand and phosphorous source.⁶ Moreover, some organic reagents containing phosphorus, such as $\text{P}(\text{SiMe}_3)_3$ or trioctylphosphine (TOP), have been used as phosphorous sources for the preparation of transition metal phosphide nanocrystals by solution phase or sol-gel methods.⁷ The phosphorous sources NaH_2PO_2 has been used in a hydrothermal-microemulsion method.¹

Nickel selenides have also attracted attention due to their interesting electrical and magnetic properties and have found applications in the field of material science. NiSe_2 is a good electrical conductor and Pauli paramagnetic metal compound. It is weakly paramagnetic with paramagnetism increasing weakly with temperature.⁸ According to the phase diagram, nickel and selenium can form a variety of nickel selenides. There are three stable phases at room temperature, Ni_{1-x}Se (the nickel content can vary from 1.00 to 0.85 relative to Se), Ni_3Se_2 and NiSe_2 , and other phases, such as Ni_2Se_3 , Ni_2Se , and Ni_3Se_4 .⁶ Nickel selenide is p-type with a band gap of 2.0 eV. Many methods have been employed for synthesis of nickel selenides, in particular

NiSe_2 , $\text{Ni}_{0.85}\text{Se}$ and Ni_3Se_2 have been prepared by solvothermal process,^{9,10} hydrothermal synthesis,^{6,11} and mechanical alloying.^{12,13} NiSe_2 and Ni_3Se_2 materials have been produced using mechanical alloying¹² starting from blended Ni and Se element powders with nominal composition $\text{Ni}_{25}\text{Se}_{75}$ and $\text{Ni}_{75}\text{Se}_{25}$, respectively. A series of nickel selenides (NiSe_2 , Ni_{1-x}Se and Ni_3Se_2) including NiSe nanowires have been synthesised through hydrothermal methods.⁶

In order to develop a route for the preparation of metal phosphide or metal selenide nanoparticles, the use of precursors in the presence of a coordinating solvent, has been investigated especially for the TOPO/TOP system.^{7,14} There are some reports on this method, for Ni-P nanoparticles, Hyeon and co-workers have used a continuous-injection method to synthesise Ni_2P nanorods by reacting the acetylacetonate $[\text{Ni}(\text{acac})_2]$ and TOP in TOPO at 330 °C.¹⁵ More recently, Senevirathne and co-workers have synthesised Ni_2P nanoparticles by using a solution-phase method with bis(1,5-cyclooctadiene) nickel(0) as the nickel source and TOP as the phosphorous source in TOPO at 345 °C.¹⁶

The use of single-source molecular precursors, which have both metal source and phosphorous/selenium source in the same structure, has been extensively studied for the synthesis of semiconductor nanoparticles. However, to the best of our knowledge, there is only one report of a single-source precursor (SSP) for nickel phosphide and/or nickel selenide nanoparticles.¹⁷ The metal complexes containing bifunctional phosphine ligands that possess alkoxy silyl functional groups were used as the precursor incorporated into silica xerogel matrixes using sol-gel chemistry. Recently, we have reported the deposition of nickel phosphide or selenide films from the single source precursor $[\text{Ni}\{{}^i\text{Pr}_2\text{P}(\text{S})\text{NP}(\text{Se})\text{Pr}_2\}_2]$ by adjusting the growth temperature in chemical vapor deposition.³

The current work employs chalcogenophosphinates as SSP for nickel selenides or nickel phosphides. This method has previously proven useful for the preparation of metal chalcogenides,¹⁸ based on the injection of dialkyldiseleno-phosphinato nickel(II) complex, $[\text{Ni}(\text{Se}_2\text{P}^i\text{Pr}_2)_2]$ (1), $[\text{Ni}(\text{Se}_2\text{P}^t\text{Bu}_2)_2]$ (2), $[\text{Ni}(\text{Se}_2\text{PPh}_2)_2]$ (3), and into hot coordinated solvents at different temperatures. Trioctylphosphine oxide (TOPO) or hexadecylamine (HDA) were used as the coordinating solvent.

The School of Chemistry and the School of Materials, The University of Manchester, Oxford Road, Manchester, UK M13 9PL. E-mail: paul.obrien@manchester.ac.uk; Fax: 44 161 275 4598; Tel: 44 161 275 4653

† CCDC reference numbers 692535 and 692536. For crystallographic data in CIF or other electronic format see DOI: 10.1039/b816903a

Experimental

Preparation of [Ni(Se₂PR₂)₂], R = 'Pr, 'Bu, Ph

A solution of NiCl₂·6H₂O (1.19 g, 5 mmol) in 5 ml MeOH was added drop wise to solution of (HNET₃)('Pr₂PSe₂) (3.77 g, 10 mmol) in 100 ml of MeOH. The mixture was stirred for 1 h at room temperature under atmospheric pressure forming green precipitate, which was filtered, washed with MeOH and re-crystallized in dichloromethane to obtain green crystals of [Ni(Se₂P'Pr₂)₂] (2.58 g, 84.75%); mp 212 °C. Elemental analysis (Found: C, 23.8; H, 4.5; P, 10.6; Ni, 9.4. Calc. for C₁₂H₂₈P₂Se₄Ni: C, 23.7; H, 4.6; P, 10.2; Ni, 9.6%; δ_H(300 MHz; CDCl₃; Me₄Si) 1.43 (dd, 36H, J 6.88 and 20.06, 6 × CH(CH₃)₂), 2.07 (dd, 6H, J 5.49 and 12.66, 6 × CH(CH₃)₂). TGA: 220–300 °C (74.01 wt% loss).

In case of [Ni(Se₂P'Bu₂)₂] and [Ni(Se₂PPh₂)₂], follow the process of making [Ni(Se₂P'Pr₂)₂] but used (HNET₃)('Bu₂PSe₂) (4.05 g, 10 mmol) and (HNET₃)(Ph₂PSe₂) (4.45 g, 10 mmol), obtained green crystals of [Ni(Se₂P'Bu₂)₂] (2.4 g, 72.2%) and dark yellow crystals of [Ni(Se₂PPh₂)₂] (3.0 g, 80.5%), respectively. For [Ni(Se₂P'Bu₂)₂], elemental analysis (Found: C, 28.7; H, 5.4; P, 9.3; Ni, 8.7. Calc. for C₁₆H₃₆P₂NiSe₄: C, 28.9; H, 5.5; P, 9.3; Ni, 8.8%; ¹H-NMR δ = 1.54 ppm (br, s, CH₃, *t*-Bu). TGA: 220–290 °C (61.14 wt% loss), 290–350 °C (5.90 wt% loss). For [Ni(Se₂PPh₂)₂], elemental analysis (found: C, 38.9; H, 2.6; P, 8.4; Ni, 7.6. Calc. for C₂₄H₂₀P₂Se₄Ni: C, 38.7; H, 2.7; P, 8.3; Ni, 7.9%). TGA: 220–350 °C (61.25 wt% loss).

Thermogravimetric analysis (TGA) measurements were performed on Seiko SSC/S200 thermal analyzer under nitrogen atmosphere from 25 °C to 500 °C at ramp of 10 °C min⁻¹.

X-Ray single crystallography

Single-crystal X-ray crystallography measurements for the compounds were collected using graphite monochromated Mo K α radiation ($\lambda = 0.71073$ Å) on a Bruker APEX diffractometer. The structure was solved by direct methods and refined by full-matrix least-squares on F^2 .¹⁹ All non-H atoms were refined anisotropically. H atoms were placed in calculated positions, assigned isotropic thermal parameters and allowed to ride on their parent carbon atoms. All calculations were carried out using the SHELXTL package.²⁰ Crystal data and structure refinement are given in Table 1. CCDC reference numbers 692535 and 692536.†

Preparation of nickel selenide and nickel phosphide nanoparticles

The method used was essentially as described by Trindade and O'Brien.¹⁸ In a typical experiment hexadecylamine, HDA (10 g) was degassed under reduced pressure at 140 °C and then heated to 330 °C under nitrogen. [Ni(Se₂P'Pr₂)₂] precursor (1.0 g) was dissolved in TOP (10 ml) and quickly injected into the hexadecylamine. The reaction temperature dropped to approximately 270 °C. The reaction mixture was heated again to 330 °C and then maintained at 330 °C for 1 h. The dark solution formed was cooled to approximately 70 °C. After cooling the reaction mixture, an excess of hot methanol was added and the solid isolated by centrifugation. The solid was washed several times with hot methanol and left to dry at room temperature. Other materials were also prepared by similar procedures. All experiments were

Table 1 Crystal data and structure refinement of [Ni(Se₂P'Pr₂)₂] (1) and [Ni(Se₂P'Bu₂)₂] (2)

Compound	[Ni(Se ₂ P'Pr ₂) ₂]	[Ni(Se ₂ P'Bu ₂) ₂]
Empirical formula	C ₁₂ H ₂₈ NiP ₂ Se ₄	C ₁₆ H ₃₆ NiP ₂ Se ₄
F_w	608.83	664.94
Temperature/K	100(2)	100(2)
Wavelength/Å	0.71073	0.71073
Crystal system	Monoclinic	Monoclinic
Space group	$P2(1)/n$	$P2(1)/c$
$a/\text{Å}$	9.2865(9)	17.8391(8)
$b/\text{Å}$	10.9349(10)	16.2638(7)
$c/\text{Å}$	10.1364(10)	33.5402(15)
$\alpha/^\circ$	90	90
$\beta/^\circ$	97.904(2)	94.1650(10)
$\gamma/^\circ$	90	90
Volume/Å ³	1019.54(17)	9705.4(7)
Z	2	16
$d_{\text{calc}}/\text{Mg m}^{-3}$	1.983	1.820
Abs. coeff./mm ⁻¹	8.236	6.930
$F(000)$	588	5216
Crystal size	0.55 × 0.55 × 0.50	0.44 × 0.25 × 0.15
Index ranges	$-11 \leq h \leq 9$, $-13 \leq k \leq 13$, $-10 \leq l \leq 12$	$-22 \leq h \leq 22$, $-20 \leq k \leq 20$, $-42 \leq l \leq 43$
Collected/unique	5643/2067	83345/23010
R_{int}	0.0216	0.0730
Data/restraints/pars.	2067/0/92	23010/0/877
Goodness-of-fit on F^2	1.074	1.009
$R_1, wR_2 [I > 2\sigma(I)]$	0.0198, 0.0470	0.0515, 0.0975
R_1, wR_2 (all data)	0.0224, 0.0479	0.0888, 0.1107
Diff. peak, hole/e Å	0.543, -0.446	1.562, -1.414

carried out at 200 °C, 280 °C and 330 °C and used both HDA and TOPO as the coordinating solvent.

Characterization of nanoparticles

The X-ray powder diffraction experiments were performed using a Bruker D8 AXE diffractometer (Cu K α). TEM samples were prepared by evaporating a drop of the material suspended in toluene onto a carbon coated copper grids. Transmission electron microscopy (TEM) was performed using a Phillips CM200 microscope at an accelerating voltage of 200 kV. High resolution transmission electron microscopy (HRTEM) was performed using Tecnai F30 FEG TEM instrument, operating at 300 kV, all samples deposited over carbon coated copper grids.

Results and discussion

Nickel phosphide and nickel selenide nanoparticles were synthesised by the thermal decomposition of [Ni(Se₂PR₂)₂] precursors, R = 'Pr, 'Bu, and Ph, in a hot surfactant solutions of TOPO or HDA. The experiments were carried out by dissolving the precursor in TOP and quickly injecting the solution into the hot TOPO or HDA at different temperatures including 200 °C, 280 °C and 330 °C. The precursors were synthesised by the deprotonation of the ligand (HNET₃)(R₂PSe₂), R = 'Pr, 'Bu, and Ph to form the anion which is then reacted with nickel(II) chloride hexahydrate in methanol to produce a dialkyldiselenophosphinato nickel(II) complex. The nanoparticles prepared from these precursors show both nickel selenide and nickel phosphide depending upon the alkyl group of the precursor, reaction temperature and capping agent.

Table 2 Nickel phosphide and nickel selenide nanoparticles accessible by reacting single source precursors for $[\text{Ni}(\text{Se}_2\text{P}^i\text{R}_2)_2]$ ($\text{R} = {}^i\text{Pr}$ (1); ${}^t\text{Bu}$ (2); and Ph (3)) with TOPO or HDA

	Reaction temperature/ $^\circ\text{C}$	Capping agent	
		TOPO	HDA
1	330	$\text{Ni}_3\text{P}(\text{hex}) + \text{Ni}_5\text{P}_4(\text{hex})$	$\text{Ni}_{12}\text{P}_3(\text{tet})$
	280	—	$\text{Ni}_{12}\text{P}_5(\text{tet})$
	200	—	—
2	330	$\text{Ni}_3\text{P}(\text{hex})$	$\text{Ni}_{12}\text{P}_3(\text{tet})$
	280	$\text{NiSe}(\text{hex})$	$\text{NiSe}(\text{hex}) + \text{NiSe}(\text{rhom})$
	200	—	—
3	330	$\text{Ni}_3\text{P}(\text{hex})$	$\text{NiSe}(\text{ortho}) + \text{Ni}_3\text{Se}_2(\text{rhom})$
	280	—	$\text{NiSe}(\text{ortho}) + \text{Ni}_3\text{Se}_2(\text{rhom})$
	200	—	—

The summary of the nanoparticles formed from this work is shown in Table 2. The decomposition reaction of the precursors was carried out at temperature 200 $^\circ\text{C}$, 280 $^\circ\text{C}$ and 330 $^\circ\text{C}$. In TOPO, Ni_3P nanoparticles were observed at 330 $^\circ\text{C}$ for all precursors except $[\text{Ni}(\text{Se}_2\text{P}^i\text{Pr}_2)_2]$ (1) which show the trace amounts of hexagonal Ni_5P_4 . NiSe nanoparticle was only formed by using $[\text{Ni}(\text{Se}_2\text{P}^i\text{Bu}_2)_2]$ (2) at 280 $^\circ\text{C}$. No deposition of nanoparticles occurred at 200 $^\circ\text{C}$ which was shown by the absence of any precipitate on addition of methanol after 1 h reaction at this temperature. This observation corresponds to the TGA results which show no decomposition at this temperature (Fig. 1). TGA showed that all complexes start decomposing at *ca.* 220 $^\circ\text{C}$. $[\text{Ni}(\text{Se}_2\text{P}^i\text{Pr}_2)_2]$ (1) and $[\text{Ni}(\text{Se}_2\text{P}^i\text{Ph}_2)_2]$ (3) decompose in one step whereas $[\text{Ni}(\text{Se}_2\text{P}^i\text{Bu}_2)_2]$ (2) decompose in two steps. The decomposition of complex (1) completes at 300 $^\circ\text{C}$ whereas the for complex (2) and (3) the decomposition completes at 350 $^\circ\text{C}$ (Fig. 1).

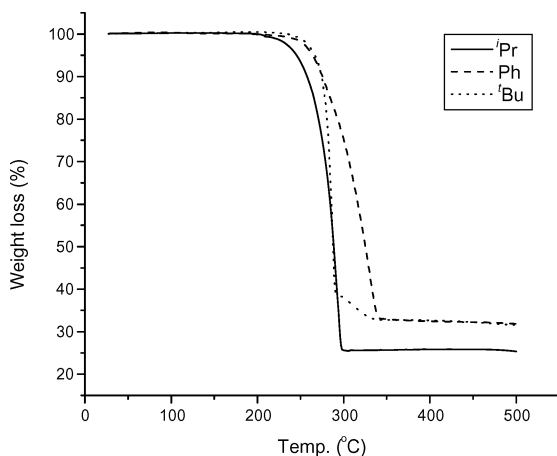


Fig. 1 TGA diagram of $[\text{Ni}(\text{Se}_2\text{P}^i\text{R}_2)_2]$ with $\text{R} = {}^i\text{Pr}$, ${}^t\text{Bu}$, Ph.

X-Ray structures

Crystallographic details and selected interatomic distances and angles of $[\text{Ni}(\text{Se}_2\text{P}^i\text{Pr}_2)_2]$ (1) and $[\text{Ni}(\text{Se}_2\text{P}^i\text{Bu}_2)_2]$ (2) are summarised in Tables 1 and 3 respectively. For $[\text{Ni}(\text{Se}_2\text{P}^i\text{Bu}_2)_2]$ (2), there are

Table 3 Selected bond distances (\AA) and the angles ($^\circ$) for $[\text{Ni}(\text{Se}_2\text{P}^i\text{R}_2)_2]$ ($\text{R} = {}^i\text{Pr}$ (1); and ${}^t\text{Bu}$ (2))

Bond distances/ \AA		Bond angles/ $^\circ$	
Compound 1			
Se(1)–P(1)	2.1703(6)	P(1)–Se(1)–Ni(1)	84.823(2)
Se(1)–Ni(1)	2.3591(3)	P(1)–Se(2)–Ni(1)	84.830(2)
Se(2)–P(1)	2.1728(6)	Se(2)–Ni(1)–Se(2A)	180.0
Se(2)–Ni(1)	2.3566(3)	Se(2)–Ni(1)–Se(1A)	90.263(9)
Ni(1)–Se(2A)	2.3566(3)	Se(2A)–Ni(1)–Se(1A)	89.736(9)
Ni(1)–Se(1A)	2.3591(3)	Se(2)–Ni(1)–Se(1)	89.737(9)
		Se(2A)–Ni(1)–Se(1)	90.264(9)
		Se(1A)–Ni(1)–Se(1)	180.0
Compound 2			
Ni(1)–Se(3)	2.3408(9)	Se(3)–Ni(1)–Se(4)	89.66(3)
Ni(1)–Se(4)	2.3467(9)	Se(3)–Ni(1)–Se(1)	90.39(3)
Ni(1)–Se(1)	2.3482(9)	Se(4)–Ni(1)–Se(1)	170.57(4)
Ni(1)–Se(2)	2.3520(9)	Se(3)–Ni(1)–Se(2)	170.77(4)
Ni(2)–Se(6)	2.3442(9)	Se(4)–Ni(1)–Se(2)	91.54(3)
Ni(2)–Se(8)	2.3473(9)	Se(1)–Ni(1)–Se(2)	89.91(3)
Ni(2)–Se(7)	2.3621(9)	Se(6)–Ni(2)–Se(8)	173.10(4)
Ni(2)–Se(5)	2.3671(9)	Se(6)–Ni(2)–Se(7)	90.53(3)
Ni(3)–Se(10)	2.3408(9)	Se(8)–Ni(2)–Se(7)	89.42(3)
Ni(3)–Se(12)	2.3499(9)	Se(6)–Ni(2)–Se(5)	89.45(3)
Ni(3)–Se(9)	2.3563(9)	Se(8)–Ni(2)–Se(5)	90.89(3)
Ni(3)–Se(11)	2.3626(9)	Se(7)–Ni(2)–Se(5)	177.60(4)
Ni(4)–Se(14)	2.3305(9)	Se(10)–Ni(3)–Se(12)	174.92(4)
Ni(4)–Se(15)	2.3396(10)	Se(10)–Ni(3)–Se(9)	89.45(3)
Ni(4)–Se(16)	2.3409(10)	Se(12)–Ni(3)–Se(9)	90.70(3)
Ni(4)–Se(13)	2.3568(9)	Se(10)–Ni(3)–Se(11)	90.44(3)
P(1)–Se(2)	2.1777(2)	Se(12)–Ni(3)–Se(11)	89.58(3)
P(1)–Se(1)	2.1809(2)	Se(9)–Ni(3)–Se(11)	178.03(4)
P(2)–Se(3)	2.1782(2)	Se(14)–Ni(4)–Se(15)	89.43(3)
P(2)–Se(4)	2.1785(2)	Se(14)–Ni(4)–Se(16)	179.13(4)
P(3)–Se(6)	2.1725(15)	Se(15)–Ni(4)–Se(16)	89.71(3)
P(3)–Se(5)	2.1792(16)	Se(14)–Ni(4)–Se(13)	89.72(3)
P(4)–Se(7)	2.1792(16)	Se(15)–Ni(4)–Se(13)	179.14(4)
P(4)–Se(8)	2.1807(16)	Se(16)–Ni(4)–Se(13)	91.14(3)
P(5)–Se(10)	2.1770(16)	P(1)–Se(1)–Ni(1)	85.24(5)
P(5)–Se(9)	2.1806(16)	P(1)–Se(2)–Ni(1)	85.22(5)
P(6)–Se(11)	2.1749(16)	P(2)–Se(3)–Ni(1)	85.90(4)
P(6)–Se(12)	2.1789(15)	P(2)–Se(4)–Ni(1)	85.75(5)
P(7)–Se(14)	2.1703(17)	P(3)–Se(5)–Ni(2)	83.38(5)
P(7)–Se(13)	2.1800(17)	P(3)–Se(6)–Ni(2)	84.07(5)
P(8)–Se(15)	2.1663(18)	P(4)–Se(7)–Ni(2)	83.25(5)
P(8)–Se(16)	2.1690(18)	P(4)–Se(8)–Ni(2)	83.56(5)
		P(5)–Se(9)–Ni(3)	83.51(5)
		P(5)–Se(10)–Ni(3)	83.96(5)
		P(6)–Se(11)–Ni(3)	83.70(5)
		P(6)–Se(12)–Ni(3)	83.91(5)
		P(7)–Se(13)–Ni(4)	84.88(5)
		P(7)–Se(14)–Ni(4)	85.74(5)
		P(8)–Se(15)–Ni(4)	85.46(5)
		P(8)–Se(16)–Ni(4)	85.37(5)
		Se(2)–P(1)–Se(1)	99.28(6)
		Se(3)–P(2)–Se(4)	98.67(6)
		Se(6)–P(3)–Se(5)	99.26(6)
		Se(7)–P(4)–Se(8)	98.91(6)
		Se(10)–P(5)–Se(9)	98.67(6)
		Se(11)–P(6)–Se(12)	99.38(6)
		Se(14)–P(7)–Se(13)	98.94(6)
		Se(15)–P(8)–Se(16)	99.19(7)

four different molecules in the asymmetric unit. The molecular structures of $[\text{Ni}(\text{Se}_2\text{P}^i\text{Pr}_2)_2]$ (1) and $[\text{Ni}(\text{Se}_2\text{P}^i\text{Bu}_2)_2]$ (2) are shown in Fig. 2.

The nickel atom is coordinated by four selenium atoms in square-planar coordination. However, the NiSe_4 plane in $[\text{Ni}(\text{Se}_2\text{P}^i\text{Bu}_2)_2]$ (2) (Fig. 2(b)) is in a distorted square planar geometry. The $\text{Se}(4)\text{--Ni}(1)\text{--Se}(1)$ and $\text{Se}(3)\text{--Ni}(1)\text{--Se}(2)$ bond

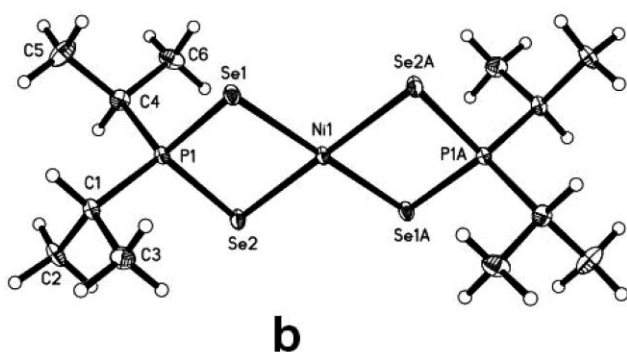
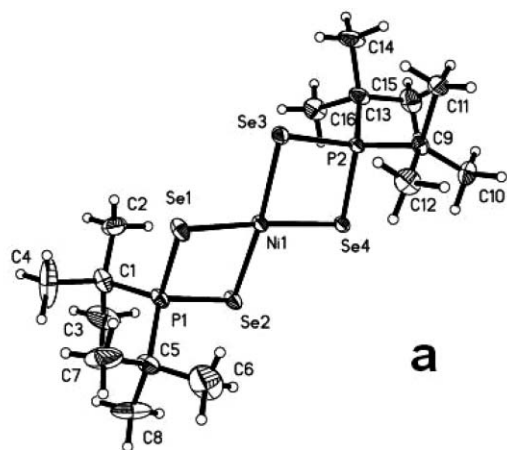


Fig. 2 ORTEP diagram showing the molecular structure of (a) the asymmetric unit of $[\text{Ni}(\text{Se}_2\text{P}'\text{Pr}_2)_2]$ (**1**) and (b) one of the four similar molecules in the asymmetric unit of $[\text{Ni}(\text{Se}_2\text{P}'\text{Bu}_2)_2]$ (**2**); thermal ellipsoids are at the 50% probability level.

angles ($170.57(4)^\circ$ and $170.77(4)^\circ$) are considerably smaller than that of $[\text{Ni}(\text{Se}_2\text{P}'\text{Pr}_2)_2]$ (**1**) (180.0°) (Fig. 2(a)). The geometry around phosphorous shows tetrahedral and the Se–P–Se bite angle is reduced in $[\text{Ni}(\text{Se}_2\text{P}'\text{Bu}_2)_2]$ due to more bulky alkyl group as in $[\text{Ni}(\text{Se}_2\text{P}'\text{Pr}_2)_2]$ (**1**). In this work, the structure of $[\text{Ni}(\text{Se}_2\text{PPh}_2)_2]$ (**3**) could not be determined because of not getting good quality crystals for X-ray study. However, the crystal structure for $[\text{Ni}(\text{Se}_2\text{PPh}_2)_2]$ (**3**) at room temperature is already reported.²¹

Characterization of nanoparticles

The crystalline nanoparticles have been characterized by using X-ray diffraction (XRD) and transmission electron microscope (TEM). Fig. 3 shows XRD patterns of the nanoparticles prepared by using TOPO as the capping agent at 330°C and 280°C . The samples show hexagonal Ni_2P (JCPDS 03-0953) and hexagonal NiSe (JCPDS 02-0892), respectively. However, the minor intermediate phase of hexagonal Ni_3P_4 was also observed from the Ni_2P nanoparticles prepared from $[\text{Ni}(\text{Se}_2\text{P}'\text{Pr}_2)_2]$ (**1**) precursor at 330°C .

Typical TEM images are given in Fig. 4. Nanoparticles with close to spherical shape are commonly observed for both Ni_2P and NiSe. The results from TEM images showed that monodispersed Ni_2P nanoparticles were obtained with an average size of 4 nm (Fig. 4(a)). The lattice fringes observed for this particle are 0.228 nm and 0.205 nm corresponding to (111) and (201) plane

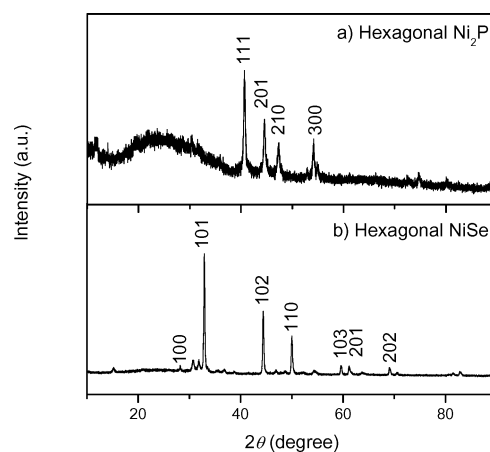


Fig. 3 XRD patterns of the particles obtained from $[\text{Ni}(\text{Se}_2\text{P}'\text{Bu}_2)_2]$ precursor in TOP/TOPO (a) 330°C (b) 280°C .

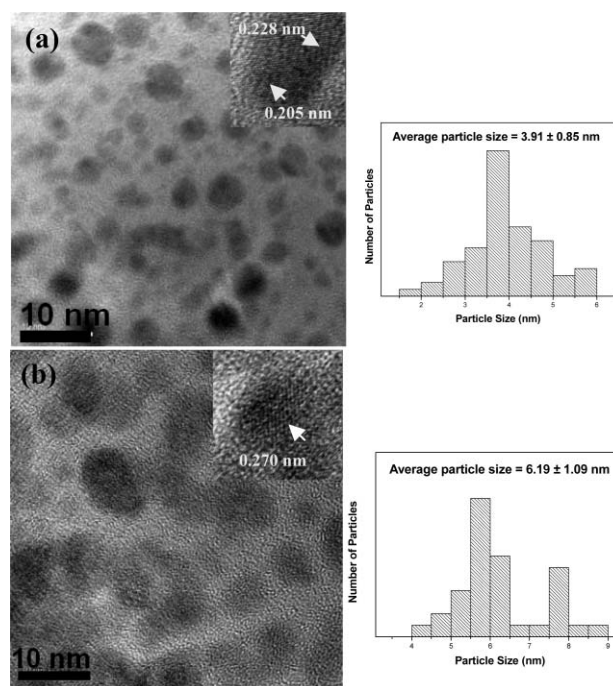


Fig. 4 HRTEM images and size distributions of (a) hexagonal Ni_2P nanoparticles obtained from $[\text{Ni}(\text{Se}_2\text{P}'\text{Bu}_2)_2]$ precursor in TOP/TOPO at 330°C ; (b) hexagonal NiSe nanoparticles obtained from $[\text{Ni}(\text{Se}_2\text{P}'\text{Bu}_2)_2]$ precursor in TOP/TOPO at 280°C .

of hexagonal Ni_2P , respectively. The NiSe nanoparticles are also generally spherical with an average size of 6.2 nm and some area of the sample also formed agglomerate of nanometric particles. The fringe spacing observed in this image is 0.270 nm corresponding to (101) plane of hexagonal NiSe (Fig. 4(b)).

In order to prove a role for TOPO in the reaction, HDA were used as an alternative capping agent under the same reaction conditions. Deposition from HDA and TOPO both gave different phases of phosphide nanoparticles for complex (**1**) whereas complex (**2**) gave phosphide as well as selenide nanoparticles. Complex (**3**) deposited only nickel selenide nanoparticles using HDA whereas the deposition from TOPO gave only phosphide (Table 2). Fig. 5 shows the XRD patterns of the stable phases

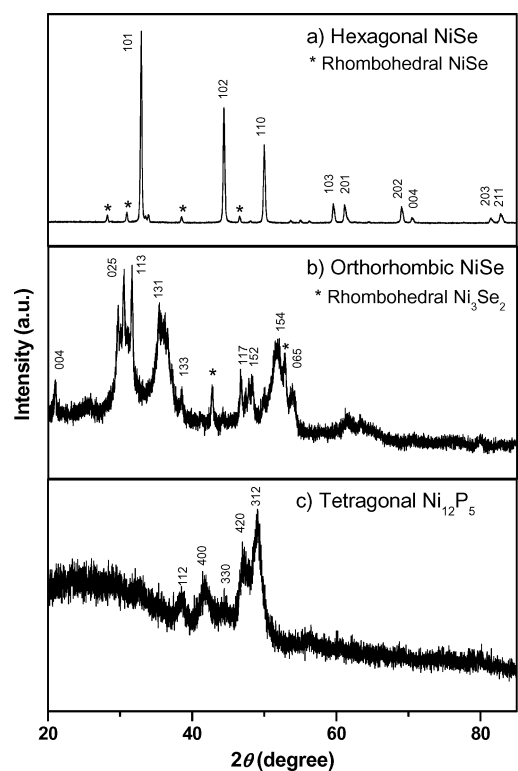


Fig. 5 XRD patterns of the particles prepared from (a) $[\text{Ni}(\text{Se}_2\text{P}^i\text{Bu}_2)_2]$ precursor; (b) $[\text{Ni}(\text{Se}_2\text{P}^i\text{Pr}_2)_2]$ precursor; (c) $[\text{Ni}(\text{Se}_2\text{PPh}_2)_2]$ precursor; all particles prepared at 280 °C by using HDA as the capping agent.

in HDA; tetragonal Ni_{12}P_5 (JCPDS 74-1381) and hexagonal NiSe (JCPDS 02-0892), as well as orthorhombic NiSe (JCPDS 29-0935). In Fig. 5(a), there are small peaks of the rhombohedral NiSe as the impurity phase. The formation of rhombohedral NiSe can be explained in terms of a competitive process between kinetic and thermodynamic control. At the beginning of the reaction, hexagonal NiSe is produced by kinetic control. When all the Se and Ni sources are consumed, the precipitation solubility process for NiSe in solution becomes the main reaction. At this time, thermodynamic control is the main factor. Longer reaction time leads to a preference for the formation of the thermodynamically stable phase. Thus, hexagonal NiSe will gradually transform into rhombohedral NiSe.⁶ The mixed phases between orthorhombic NiSe and rhombohedral Ni_3Se_2 were also observed by using $[\text{Ni}(\text{Se}_2\text{P}^i\text{Pr}_2)_2]$ (I) precursor (Fig. 4(b)). The XRD patterns show orthorhombic NiSe as the major phase with small amount of rhombohedral Ni_3Se_2 .

Typical TEM images for these samples are shown in Fig. 6. All samples are nearly spherical in shape. Fig. 6(a) shows monodispersed Ni_{12}P_5 nanoparticles with an average size of 5.6 nm. The lattice spacing observed in the image is 0.216 nm corresponding to 400 planes of tetragonal Ni_{12}P_5 . Spherical nanoparticles of hexagonal NiSe show in Fig. 6(b). The average particle size is 6.6 nm. The lattice fringes show a *d*-spacing of 0.203 nm which corresponds to the 102 plane. In case of orthorhombic NiSe, the nanoparticles are also generally spherical with an average size of 5.1 nm; in some areas of the image agglomerates of nanomeric particles are also formed. The lattice spacing observed in this image is 0.155 nm corresponding to 103 plane of hexagonal NiSe (Fig. 6(c)).

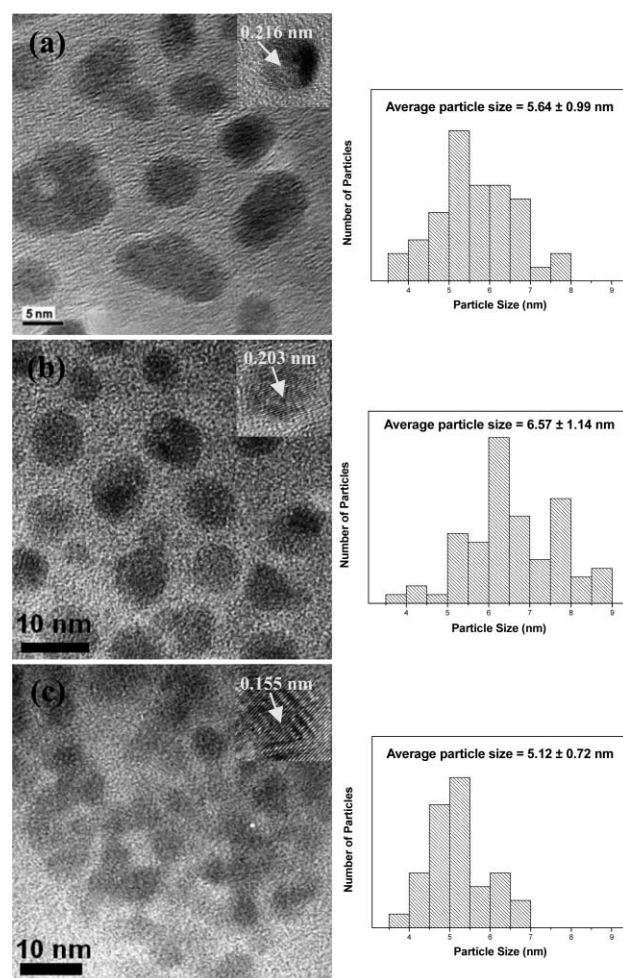


Fig. 6 HRTEM images and size distribution of (a) tetragonal Ni_{12}P_5 obtained from $[\text{Ni}(\text{Se}_2\text{PPh}_2)_2]$ precursor; (b) hexagonal NiSe obtained from $[\text{Ni}(\text{Se}_2\text{P}^i\text{Bu}_2)_2]$ precursor; (c) the orthorhombic NiSe obtained from $[\text{Ni}(\text{Se}_2\text{P}^i\text{Pr}_2)_2]$ precursor; all samples prepared at 280 °C by using HDA as the capping agent.

In this work, we generally observed that higher temperatures tend to favour the deposition of nickel phosphide nanoparticles probably because of either higher phosphorous availability or *via* TOP decomposition.^{22–24} However, the product also depends on the nature of the single source precursor, for instance, $[\text{Ni}(\text{Se}_2\text{PPh}_2)_2]$ (3) only formed NiSe. Moreover, the coordinating solvents including TOPO and HDA play an important role in the chemical composition of nickel phosphide nanoparticles. Whilst, the richer phosphorous phase Ni_2P (P:Ni = 0.5) was always formed when using TOPO as the capping agent, the phase Ni_{12}P_5 (P:Ni = 0.42) was formed when using HDA as the capping agent.

Conclusions

In this paper, we have shown that nickel phosphide and nickel selenide nanoparticles can be synthesised in a one pot reaction using single source molecular precursors of the type $[\text{Ni}(\text{Se}_2\text{PR}_2)_2]$, (R = *i*Pr, *t*Bu, or Ph) in coordinating solvent such as TOPO and HDA at moderate temperatures. The chemical compositions of the nanoparticles can easily be controlled by varying temperature, capping agent, and type of precursor. The monodispersed

nanoparticles prepared from this method are spherical in shape. The nanoparticles can be formed at low temperatures ($<370\text{ }^{\circ}\text{C}$), which represents an alternative, convenient and simple route to synthesise nickel selenide or phosphide nanoparticles.

Acknowledgements

WM would like to acknowledge the Royal Thai Government for funding. The authors also thank EPSRC, UK for financial assistance.

Notes and references

- 1 Y. Ni, A. Tao, G. Hu, X. Cao, X. Wei and Z. Yang, *Nanotechnology*, 2006, **17**(19), 5013.
- 2 A. I. Zaitsev and N. E. Zaitseva, *Dokl. Phys. Chem.*, 2002, **387**, 295.
- 3 A. Panneerselvam, M. A. Malik, M. Afzaal, P. O'Brien and M. Helliwell, *J. Am. Chem. Soc.*, 2008, **130**, 2420.
- 4 H. L. Su, Y. Xie, B. Li, X. M. Liu and Y. T. Qian, *Solid State Ionics*, 1999, **122**, 157.
- 5 S. Yang and R. Prins, *Chem. Commun.*, 2005, 4178.
- 6 Z. Zhuang, Q. Peng, J. Zhuang, X. Wang and Y. Li, *Chem. Eur. J.*, 2006, **12**, 211.
- 7 C. Qian, F. Kim, L. Ma, F. Tsui, P. Yang and J. Liu, *J. Am. Chem. Soc.*, 2004, **126**(4), 1195.
- 8 Z. Meng, Y. Peng, L. Xu and Y. Qian, *Chem. Lett.*, 2001, **30**(8), 776.
- 9 Z. H. Han, S. H. Yu, Y. P. Li, H. Q. Zhao, F. Q. Li, Y. Xie and Y. T. Qian, *Chem. Mater.*, 1999, **11**, 2302.
- 10 Q. Lu, J. Hu, K. Tang, B. Deng, Y. Qian, G. Zhou and X. Liu, *Mater. Chem. Phys.*, 2001, **69**, 278.
- 11 X. Liu, G. Qiu, J. Wang and Y. Li, *Chem. Lett.*, 2004, **33**, 852.
- 12 C. E. M. Campos, J. C. Lima, T. A. Grandia, K. D. Machado, P. S. Pizani and R. Hinrichs, *Solid State Ionics*, 2004, **168**, 205.
- 13 A. Zhao, L. Xu, T. Luo and Y. Qian, *Chem. Lett.*, 2005, **34**, 1136.
- 14 S. L. Brock, S. C. Perera and K. L. Stamm, *Chem. Eur. J.*, 2004, **10**(14), 3364.
- 15 J. Park, B. Koo, K. Y. Yoon, Y. Hwang, M. Kang, J. G. Park and T. Hyeon, *J. Am. Chem. Soc.*, 2005, **127**, 8433.
- 16 K. Senevirathne, A. W. Burns, M. E. Bussell and S. L. Brock, *Adv. Funct. Mater.*, 2007, **17**, 3933.
- 17 C. M. Lukehart and S. B. Milne, *Chem. Mater.*, 1998, **10**(3), 903.
- 18 T. Trindade and P. O'Brien, *Adv. Mater.*, 1996, **8**, 161.
- 19 G. M. Sheldrick, *SHELXS-97, Program for solution of crystal structures*, University of Göttingen, Germany, 1997; G. M. Sheldrick, *SHELXL-97, Program for refinement of crystal structures*, University of Göttingen, Germany, 1997.
- 20 Bruker, *SHELXTL Version 6.12*, Bruker AXS Inc., Madison, Wisconsin, USA, 2001.
- 21 L. Gastaldi and P. Porta, *Cryst. Struct. Commun.*, 1977, **6**(2), 175.
- 22 S. C. Perera, G. Tsoi, L. E. Wenger and S. L. Brock, *J. Am. Chem. Soc.*, 2003, **125**, 13960.
- 23 A. E. Henkes and R. E. Schaak, *Chem. Mater.*, 2007, **19**(17), 4234.
- 24 Y. Li, M. A. Malik and P. O'Brien, *J. Am. Chem. Soc.*, 2005, **127**(46), 16020.